ADVANCED ELECTRONIC MATERIALS
www.advelectronicmat.de

Highly Bendable and Stretchable Electrodes Based on Micro/Nanostructured Gold Films for Flexible Sensors and Electronics

*Yujie Zhu and Jose Moran-Mirabal**

Simple and inexpensive ways of fabricating electronics on flexible substrates are in high demand for wearable devices,[1] sensors,[2] and actuators,[3] where conductive materials need to perform consistently under strain.[4] To date, various nanomaterials, such as polymers,[5] carbon nanotubes,[6] graphene,[7,8] metal films,[9] and nanoparticles,[10,11] have been used as flexible conductors. However, most of these materials are limited in their applicability due to instability, low conductivity, or high material cost.[12] Thus, simple and cost-effective methods to make stretchable electrodes from metal films are highly desirable. Metal films can be structured to achieve stretchability through: 1) patterning thin films into spring-shape wires[13] or filament networks;[14] 2) introducing roughness at a metal/elastomer interface to produce nonpercolating cracks during stretching;[15] 3) using pre-stressed elastomeric substrates during thin film deposition followed by strain release.[9] The first strategy involves expensive and complex fabrication processes, while the other methods are limited in the maximum strain that the electrodes can withstand. In this manuscript, by combining shape-memory polymer shrinking[16–18] with patterning through xurography[19,20] and lift-off, we introduce a simple and inexpensive method for fabricating structured metal electrodes. Such electrodes exhibit excellent conductivity, electrochemical sensing stability, and great resiliency to stretching and bending strain on poly(dimethylsiloxane) (PDMS) and Ecoflex elastomeric substrates.

The bench-top fabrication of stretchable conductive films is illustrated in **Figure 1**A. Adhesive vinyl served as a mask during gold deposition to create centimeter to sub-millimeter patterned electrodes. After vinyl lift-off, the polystyrene substrate (PS) was shrunk down to ≈16% of its original size, resulting in micrometer size electrodes. Additionally, the shrinking process buckled and wrinkled the gold films, resulting in micro/nanostructured surfaces. The structured films were lifted off by dissolving an intermediate photoresist layer, whose thickness was optimized to yield small micro/nanostructures on the gold film and to allow it to be readily lifted off (Figure S1, Supporting Information). The last fabrication step involved transferring the gold film to the receiving substrate. Figure 1B,C shows photos of structured gold films (200 nm-thick) transferred onto PDMS and SiO_2 substrates, respectively. To achieve the best adhesion on the receiving elastomers (PDMS/Ecoflex), they were partially cured prior to the transfer of the structured metal films. It was observed that the presence of bubbles or contaminants at the gold/elastomer interface led to film delamination, resulting in low electrode stretchability. Using the optimized conditions, this simple and inexpensive benchtop method allowed the patterning, structuring, and transferring of thin gold films.

The structured films were characterized through electron and optical microscopy before and after the lift-off and the transfer to the receiving substrates. Scanning electron microscopy (Figure 1D) showed that 20 nm-thick films presented smaller structures than 200 nm ones, because thinner films buckled more readily during shrinking.[21] Little difference was observed in the morphology for the structured films before lift-off, after lift-off, and after transfer onto elastomer substrates. To confirm this observation, the surface roughness of the structured films was measured through optical profilometry. The surface root mean squared roughness was measured to be statistically equal before lift-off, after lift-off, and after transfer to the receiving substrates (Figure S2, Supporting Information). This shows that the fabrication process does not change the physical attributes of the structured films.

To test the stretchability of structured Au/PDMS electrodes, their conductivity was tested under strain. The structured electrode resistance was measured in a two-probe setup (**Figure 2**A, bottom inset) at 5% strain increments. Typical I–V curves at 0%, 50%, and 100% strain are shown in the top inset of Figure 2A. All electrodes remained conductive until the PDMS failed mechanically (110%–130% strain), suggesting that they are excellent candidates for PDMS-based devices. The effect of electrode shape on stretchability was assessed by measuring the conductivity under strain for electrodes with different form factors (defined as length-to-width ratio, L/W, Figure 2A). As L/W increased, the resistance at comparable strains also increased. This is explained by film cracking perpendicular to the stretching axis, which reduces the number of available conductive paths. For electrodes with high L/W, the number of cracks necessary to span the width of the electrode, resulting in a total loss of conductivity, is smaller than for electrodes with low L/W. This is exemplified by Figure 2A, where the resistance for electrodes with W = 2, 0.8, and 0.8 mm and L/W = 3, 5, and 7.5 at 100% strain is, on average, ≈10%, ≈30%, and ≈100% higher than their initial (relaxed) resistance. Thus, electrodes with large form factors could be useful as strain sensors, while those with small form factors would be robust conductive elements for applications where a constant resistance is required.

Y. Zhu, Prof. J. Moran-Mirabal
Department of Chemistry and Chemical Biology
McMaster University
1280 Main Street West, Hamilton,
ON L8S 4M8, Canada
E-mail: mirabj@mcmaster.ca

DOI: 10.1002/aelm.201500345

ADVANCED ELECTRONIC MATERIALS
www.advelectronicmat.de

Materials Views
www.MaterialsViews.com

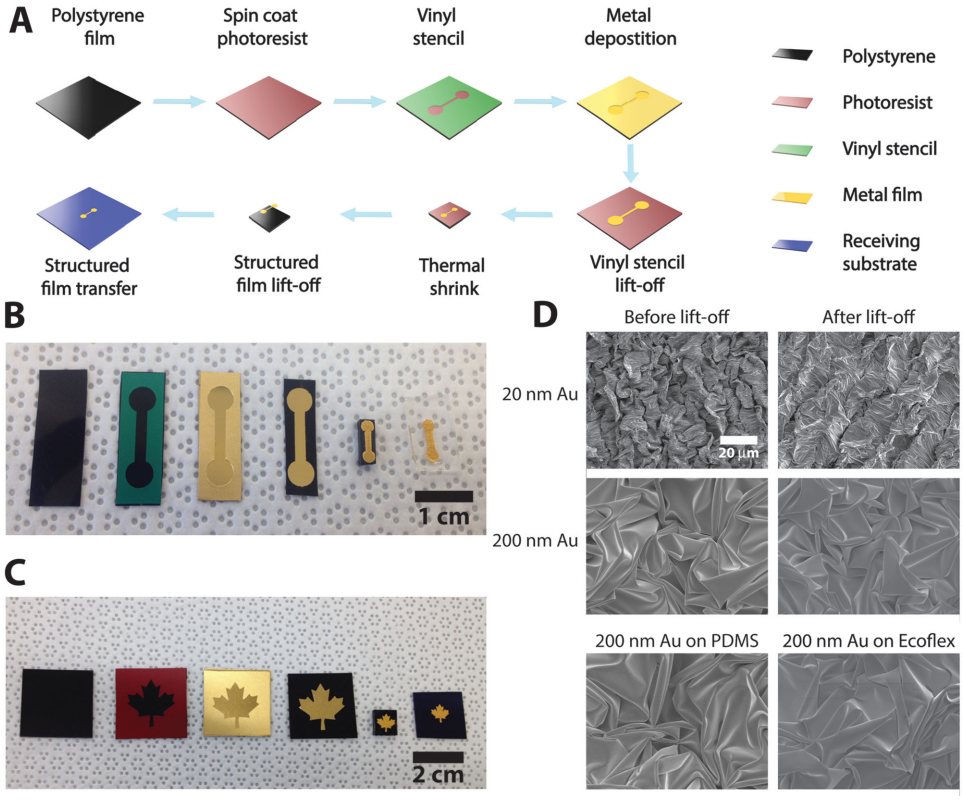

Figure 1. Fabrication of structured electrodes. A) Schematic of the bench-top micro/nanostructured metal thin film fabrication and transfer. B) Depiction of the fabrication process of gold electrode transferred on to PDMS. C) Depiction of the fabrication of patterned maple leaf-shaped Au film and the transfer onto a silicon wafer. D) SEM images of 200 nm Au films before and after lift-off, and after transfer to PDMS. SEM images were taken with accelerating voltage of 2.5 kV, working distance of 6 mm, and low probe current. All images taken at the same magnification.

To overcome the limitations of PDMS-based devices and explore the maximum stretchability of micro/nanostructured electrodes, we used Ecoflex elastomer as the receiving substrate (≈800% elongation at break). Resistance measurements under strain for Au/Ecoflex electrodes ($L/W = 7.5$, Figure 2B) showed higher interdevice variability than those on PDMS. This is a result of the variability in adhesion between the film and elastomer, where areas of the film that did not adhere well delaminated more easily. The measured strain at conductivity break was 135%, with the relative resistance remaining in the range of 1–2.5 for strains up to 130% (Figure 2B). As controls, we tested the conductivity of planar gold electrodes fabricated directly on the elastomer surfaces. The flat Au/elastomer films cracked and delaminated much more readily (Figure S3, Supporting Information), losing conductivity with little applied strain (<5%). These results highlight the need for a structured film and proper adhesion to obtain highly stretchable and conductive electrodes.

Biaxial stretchability is required for conductive elements that can be draped over arbitrary surfaces. Various materials with such properties have been explored in the past, including silver nanowires,[22] gold,[9] and graphene films.[23] To test the biaxial stretchability of structured Au/PDMS electrodes, their conductivity was evaluated under strains along two orthogonal axes. For a design with $L/W = 1$ (Figure 2C), the relative resistance experienced little variation when 0%–50% strain was applied along orthogonal axes. The uniform behavior when the micro/nanostructured gold films are stretched biaxially suggests that they could be attractive as electrodes attached to the surface of inflatable devices (e.g., balloon catheters).[24]

To understand the stretching mechanics of micro/nanostructured Au/PDMS electrodes, their surfaces were imaged under strain. From reflected and transmitted light microscopy images (Figure 2D), it can be seen that the wrinkles on the structured gold films contribute to their enhanced stretchability in two ways. First, the wrinkles unfold as the film is stretched, which maintains the integrity of the film by keeping the tensile stress low. Second, the cracks that originate from the weakest points or defects on the film extend along the wrinkles as the strain increases. The random orientation of the wrinkles prevents cracks from propagating across the film and minimizes the loss of conductivity. Finally, micro/nanostructure size and periodicity do not impact film stretchability and conductivity, as shown by electrodes fabricated from films with different thicknesses (Figure S4, Supporting Information). These experiments show that the stretchability of structured electrodes derives from features produced during the shrinking process, and hints at alternative methods that exploit surface structuring for the fabrication of flexible devices.

The implementation of flexible electronics also requires that the conductivity be reproducible under stretching and bending. To assess reproducibility, changes in resistance were

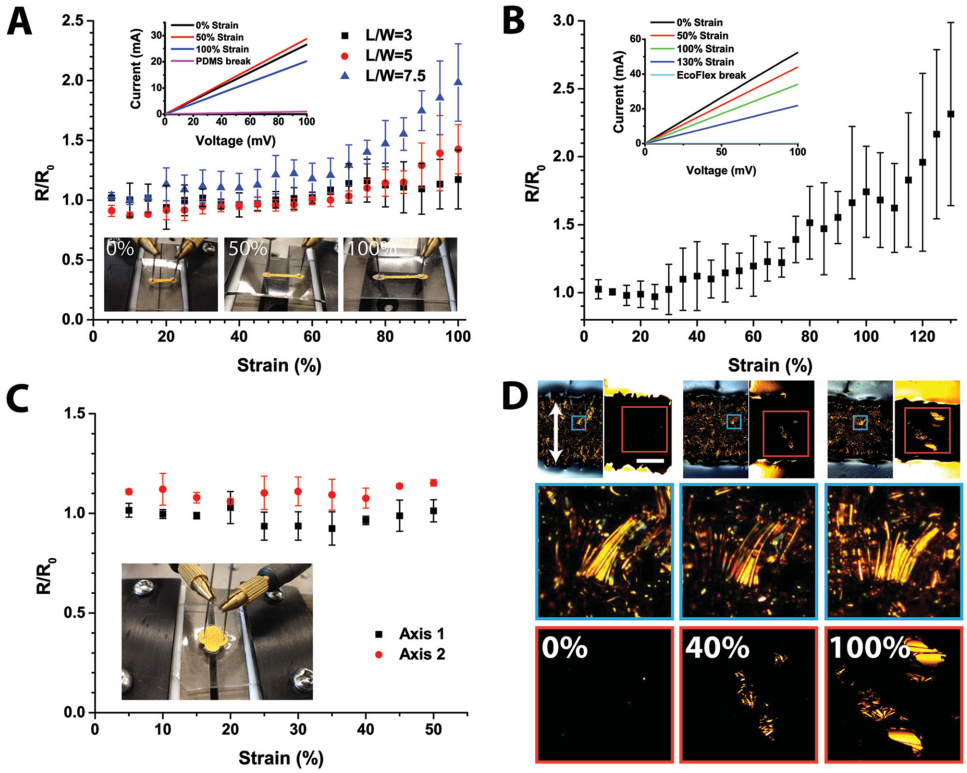

Figure 2. Stretchability and mechanism. A) Relative resistance change measurement under various strains for stretchable electrodes on PDMS substrates with $L/W = 3$ (black square, $W = 2$ mm), 5 (red circle, $W = 0.8$ mm), and 7.5 (blue triangle, $W = 0.8$ mm). Top inset graph shows typical I–V curves where resistance was extracted for gold electrodes ($L/W = 5$) under 0%, 50%, 100% strains and when PDMS broke. Bottom inset photos show the two-probe measurement for a gold electrode/PDMS device under 0%, 50%, and 100% stretching strain, respectively. B) Relative resistance change measurement under various strains for gold electrode ($L/W = 3$, $W = 2$ mm) on Ecoflex substrate. The electrode lost conductivity at 135% strain. Insets represent I–V curves for gold electrode stretched on Ecoflex at 0%, 50%, 100%, 130%, and 135% strain (conductivity broke). C) Biaxial stretchability. The relative resistance change shows the same trend when Au/PDMS device was stretched along two orthogonal axes, indicating similar electric properties of both axes. Inset is a photo of flower-shaped Au film on PDMS at 0% strain for biaxial stretching measurement. D) Optical images show gold film morphology change during the stretching process. The top row shows reflected (left panels) and transmitted light (right panels) images that reveal the unwrinkling and cracking process of the gold film. The scale bar in this image is 500 μm. The areas confined with blue (reflected light) and red (transmitted light) squares were zoomed into for clearer observation. The reflected light images (middle row, blue) reveal the unwrinkling of surface features when tensile stress (0%, 40%, 100%) is applied. On the other hand, the transmitted light images (bottom row, red) show the evolution of defects or cracks in the gold film as tensile stress (0%, 40%, 100%) is applied.

measured for Au/elastomer devices ($W = 0.8$ mm, $L/W = 7.5$) over 100 stretching and bending cycles. On PDMS, the resistance measurements were done at 0% and 50% strain (**Figure 3**A). Over the first two cycles, resistance increased slightly at 50% strain, which was attributed to the development of the necessary cracks to relieve tensile strain. After the initial "conditioning" of the electrodes, resistance remained constant for the stretched and relaxed states. Similarly, Ecoflex devices were tested at 0% and 100% strain (Figure 3B), where the relative resistance under strain remained constant at 1.4 for the first 20 cycles, and increased to 2.1 over the next 80 cycles. This increase is attributed to partial delamination due to the weaker adhesion of the structured film to Ecoflex. It must be noted, however, that the increase is among the lowest reported in the literature for metallic film or nanostructure-based stretchable conductors.[25,26] To determine if electrodes stretched beyond their break point could recover conductivity upon relaxation, we measured the resistance for Au/Ecoflex devices released from 150% strain (beyond conductivity break point, Figure 3C). No significant change occurred until after the 80th cycle and the relative resistance only increased to 1.45 through the 100th cycle. Similar behavior was observed for a device stretched to 100% strain (Figure 3B), which indicates that the Au/Ecoflex electrodes remain conductive but exhibit slight degradation after ≈80 cycles.

The reproducibility in conductivity of Au/PDMS structured electrodes after bending was also investigated. Bending was performed by wrapping the Au/PDMS device around a Teflon mold with known radius of curvature (Figure 3C, $r = 5$, 2.5, or 1 mm, corresponding to tensile strains at the film of 12%, 24%, or 60%, respectively) and releasing it, after which the resistance was measured. Figure 3C shows the relative resistance of Au/PDMS electrodes ($W = 0.8$ mm, $L/W = 7.5$) over 100 bend and release cycles. Even for the highest strain (60%, $r = 1$ mm) the conductivity fully recovered after the release, and remained unchanged over 100 cycles. These results, coupled with those from stretching experiments, showcase the robustness of the micro/nanostructured electrodes, which retain excellent conductivity over repeated stretching and bending cycles.

ADVANCED ELECTRONIC MATERIALS
www.advelectronicmat.de

Materials Views
www.MaterialsViews.com

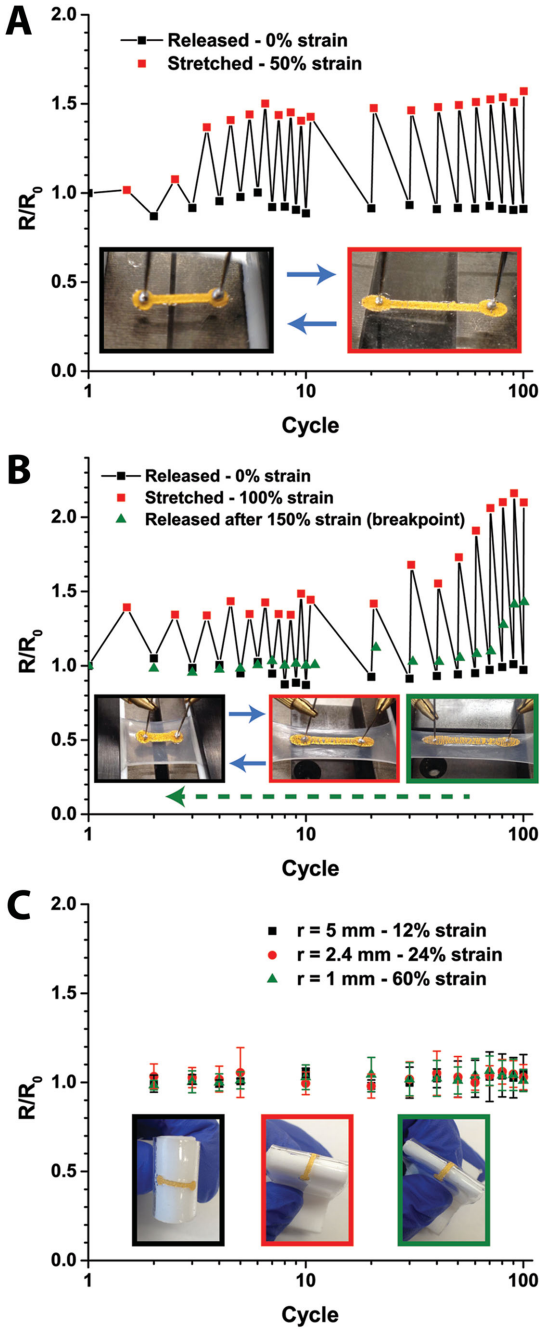

Figure 3. Stretching and bending reproducibility. A) Relative resistance of an Au/PDMS electrode ($W = 0.8$ mm, $L/W = 7.5$) stretched from 0% to 50% strain over 100 stretching cycles. Inset photos show the device at 0% (black, left inset photo) and 50% strain (red, right inset photo). B) Relative resistance of Au/Ecoflex electrode ($W = 2$ mm, $L/W = 3$) over 100 stretching cycles from 0% (black, left inset photo) to 100% (red, middle inset photo) strain, as well as relative resistance of devices after being stretched beyond their conductivity break point (≈150% strain) and released back to 0% strain (green, right inset photo). C) Relative resistance of Au/PDMS electrodes ($W = 0.8$ mm, $L/W = 7.5$) released after being bent to 12% (black, left inset photo), 24% (red, middle inset photo), and 60% (green, right inset photo) bending strains. Inset photos show the electrode bent along holders with radii of 5 (black), 2.5 (red), and 1 mm (green). Each stretching and bending test was performed with three replicate electrodes.

As proof-of-concept of the use of structured gold films as conductive elements in functional devices, they were used as flexible electrodes for electrochemical sensing. First, cyclic voltammetry (CV) was used to measure the electroactive surface area (ESA) of devices at different fabrication stages: planar films on PS, structured films after shrinking, free-standing structured films after lift-off, and structured films transferred onto PDMS (**Figure 4**A). CV was performed using the films as the working electrode in a three-electrode electrochemical cell (Figure 4B, inset). The voltammograms displayed well-defined peaks associated with the oxidation/reduction of the gold surface. By quantifying the total charge transferred, the ESA of each film was assessed. Structured films on PS exhibited an increase in ESA (≈520%) that is consistent with the reduction in the device footprint produced through shrinking. After lift-off, the ESA of the free standing films increased by 80%. This was less than the 100% increase expected, which was attributed to photoresist or polystyrene residues left on the backside of the film after lift-off (Figure S5, Supporting Information). Conversely, the ESA of films transferred onto PDMS was statistically equal to that of the films before lift-off. This showed that the surface of the structured films transferred onto PDMS substrates was not damaged by the fabrication procedure and could be suitable for electrochemical measurements.

Structured Au/PDMS electrodes were used for electrochemical sensing with and without external bending strain. A circular working electrode and two arc-shaped counter electrodes were fabricated on PDMS (Figure 4B, inset photo) and an external Ag/AgCl electrode was used as reference. Chronoamperometry was used to assess the electrodes' response to different concentrations of redox-active molecules (ferrocyanide and ascorbic acid (AA)) in aqueous solutions. In all electrochemical-sensing experiments, the current was normalized to the current measured for the highest concentration, to account for any device-to-device variability. Figure 4B shows that current is linearly proportional to ferrocyanide concentrations from 50×10^{-6} M to 100×10^{-3} M for electrodes under 0% and 30% bending strain, where they also exhibited similar performance and limit of detection (50×10^{-6} M). With a geometric area of the structured electrode of 0.196 cm^2, the sensitivity was calculated to be 0.05×10^{-3} M^{-1} cm^{-2} for relaxed and strained sensors. We further investigated the electrode response to temporal changes in AA concentration. Figure 4C shows typical chronoamperograms for structured gold electrodes (held at a constant potential of 0.4 V) in response to temporal increases of AA concentration. AA calibration curves constructed from three replicate devices show excellent linearity in the 10×10^{-6} M -5×10^{-3} M concentration range for relaxed ($I/I_{max} = 0.2027 \times C_{AA} + 5 \times 10^{-5}$, $R^2 = 0.9999$) and strained electrodes ($I/I_{max} = 0.2007 \times C_{AA} + 0.0034$, $R^2 = 0.9994$). Furthermore, the relaxed and bent devices had identical limit of detection (20×10^{-6} M), while strain caused only a 1% decrease in sensitivity (from 1.03 M^{-1} cm^{-2} for relaxed to 1.02×10^{-3} M^{-1} cm^{-2} for strained devices). These results show that the structured electrodes are suitable for applications where flexibility or stretchability of the conductive elements is required, such as in flexible electrochemical sensors.

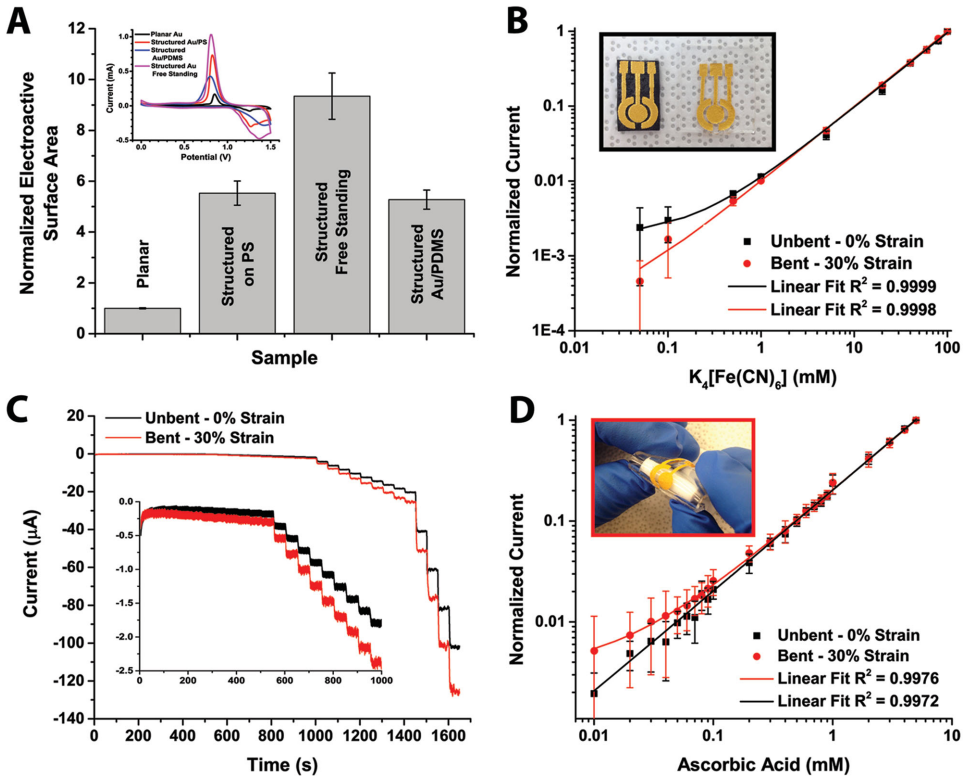

Figure 4. Electrochemical characterization and sensing. A) Electroactive surface area measurement through cyclic voltammetry for planar gold films, structured gold films on polystyrene, structured gold films after transfer onto PDMS, and structured free-standing gold films. Inset graph is a comparison of cyclic voltammograms of each type of samples obtained in 0.05 M acid solutions. B) Calibration curves of response current over potassium ferrocyanide concentration in chronoamperometric measurements performed with unbent (0% strain) and bent (30% strain) Au/PDMS sensing devices. C) Typical amperometric curves of unbent (0% strain) and bent (30% strain) sensors to successive addition of ascorbic acid (final concentrations from 1 μm to 5×10^{-3} M) in 0.02 M phosphate buffer solution (pH 7.0) at a constant applied potential of 0.4 V. D) Calibration curves of the current response over ascorbic acid concentration for both unbent and bent (30% strain) devices. Error bars represent the standard deviation of measurements performed on a minimum of at least three using different devices.

In conclusion, we have demonstrated a simple, rapid, and inexpensive technique to fabricate highly stretchable micro/nanostructured metal electrodes. By combining shape-memory polymer shrinking and thin film lift-off, we successfully fabricated and transferred micro/nanostructured gold electrodes onto stretchable elastomeric substrates. Little change was observed in the conductive properties of Au/PDMS devices under strain until the substrate mechanically failed, while the Au/Ecoflex devices remained conductive up to 135% strain. Furthermore, the structured electrodes showed uniform properties when stretched along two orthogonal axes. It was observed that the micro/nanostructured surface contributed to the stretchability of the electrodes in two ways: releasing tensile stress by unfolding of the wrinkles and preventing crack propagation by the random orientation of the wrinkles. The structured electrodes also displayed resilience to bending strains, as demonstrated by the complete recovery of their initial conductivity from tensile strains of up to 60%. Finally, the structured electrodes also proved to be candidates for flexible electrochemical sensors, as they performed very similarly in the detection of redox active molecules with and without applied strain. We anticipate that such micro/nanostructured electrodes could find use as conductive elements in flexible, stretchable, and/or inflatable electronics and sensors.

Experimental Section

Pre-stressed polystyrene films (Graphix Shrink Film, Graphix, Maple Heights, Ohio) were cleaned and spin coated with positive photoresist of thicknesses ranging from 100 to 1.8 μm. After being heated at 90 °C for 3 min to remove residual solvent, the sheets were covered with self-adhesive vinyl (FDC-4300, FDC graphic films, South Bend, Indiana), and the desired shapes were cut out using a vinyl cutter (Robo Pro CE5000-40-CRP, Graphtec America Inc., Irvine, California). Gold was deposited from 99.999% purity gold target (LTS Chemical Inc., Chestnut Ridge, New York) using a Torr Compact Research Coater CRC-600 manual planar magnetron sputtering system (New Windsor, New York) onto the masked shrink film. After removing the vinyl mask, gold coated polystyrene films were shrunk at 160 °C. The metal films were lifted off from the substrates by dissolving the photoresist in acetone. The lifted-off gold films were then washed and transferred onto partially cured silicone elastomers, Sylgard-184 PDMS and Ecoflex rubber, which were then cured to completion. Addition of methanol helped to overcome the electrostatic repulsion between PDMS and gold surfaces, thus making it easier to lay down the structured gold films.

The surface morphology of the gold thin films before and after lift-off was characterized using a JEOL JSM-7000S Scanning Electron Microscope with an accelerating voltage of 2.5 kV, working distance of 6 mm, and low probe current. An estimate of surface roughness by the root mean square (RMS) and peak-to-valley (PV) values was obtained using a Zygo NewView 5000 white light interferometry microscope (Zygo Corporation, Middlefield, Connecticut). The electrochemically active surface area of the gold films before shrinking, after shrinking on

polystyrene, and transferred onto PDMS, was measured by CV using a CHI 660D Electrochemical Workstation (CH Instrument, Austin, Texas). A standard three-electrode setup was used for electrochemical sensing, with the fabricated structured electrodes as working and counter electrodes, and an Ag/AgCl electrode as reference electrode. CV scans were performed in 0.05 M H_2SO_4 at a scan rate of 0.1 V^{-1} s^{-1} and a voltage range between 0 and 1.5 V. Self-adhesive vinyl films with a single 0.5 cm by 0.5 cm square cut out were used as masks to expose the same geometric surface area (0.25 cm^2) of the gold films. The reduction peak of the resulting cyclic voltammograms was integrated to determine the charge and the electrochemically active surface area was calculated (Surface area = charge/surface charge density) using the surface charge density of a monolayer of gold, 386 μC cm^{-2}.

2-probe resistance measurements were performed on gold film electrodes using a source picoammeter (Model 2450, Keithley Instruments, Cleveland, Ohio). A droplet of eutectic gallium-indium (EGAIn, Sigma-Aldrich, St. Louis, Missouri) was used to create better contact between the Pt-wire probes and the structured gold films. The source voltage was swept linearly from 0 to 100 mV in 10 mV steps, and the resulting current was measured. *I–V* curves were recorded, and resistance *R* was extracted using $R = \Delta V/\Delta I$. The Au/PDMS and Au/Ecoflex electrodes were stretched on a home-built stretcher in 5% strain increments and resistance was measured at each strain level. The film resistance was obtained at 3–6 probe positions and compared across a minimum of three replicate devices. Bending measurements were carried out using custom machined Teflon holders with radii of 5, 2.5, and 1 mm. Resistance was measured over 100 cycles of stretching and bending. The stretching process of micro/nanostructured gold film was imaged using Nikon Eclipse LV100N POL epifluorescence microscope (Nikon Instruments, Mississauga, Ontario) equipped with a Nikon 4×/0.10NA objective. Reflected and transmitted light images were taken from the gold electrode while it was being stretched from 0% to 100% strain at a 10% strain interval. All these images were acquired with an Infinity 1 color camera (Lumenera, Ottawa, Ontario) and recorded with Infinity Capture software (Lumenera).

The flexible electrodes were used as working and counter electrodes to detect concentrations of potassium ferrocyanide and ascorbic acid electrochemically. An Ag/AgCl electrode was used as reference electrode in a three-electrode system. $K_4Fe(CN)_6$ solutions from 50×10^{-6} M to 100×10^{-3} M were measured by chronoamperometry at a fixed potential of 0.5 V for 1 s. 1 M KCl was used as the supporting electrolyte. For AA detection, all chronoamperometric measurements were performed at 0.4 V in 1 × PBS (100×10^{-3} M, pH = 7.4). The transient background current was allowed to decay to a steady-state value before the addition of AA from 1×10^{-6} M to 5×10^{-3} M. The solution was stirred to provide convective transport.

Supporting Information

Supporting Information is available from the Wiley Online Library or from the author.

Acknowledgements

This research was supported by the Natural Sciences and Engineering Research Council (NSERC, RGPIN/418326) and a Canada Foundation for Innovation Leaders Opportunity Fund. Y.Z. was partially supported by an NSERC IDEM CREATE Grant. J.M.-M. was the recipient of the Early Researcher Award through the Ontario Ministry of Research and Innovation. This research made use of instrumentation available through the BioInterfaces Institute and Canadian Centre for Electron Microscopy at McMaster University.

Received: October 13, 2015
Revised: December 07, 2015
Published online: January 19, 2016

[1] M. Stoppa, A. Chiolerio, *Sensors* **2014**, *14*, 11957.
[2] A. Chortos, Z. Bao, *Mater. Today* **2014**, *17*, 321.
[3] U. Kim, J. Kang, C. Lee, H. Y. Kwon, S. Hwang, H. Moon, J. C. Koo, J.-D. Nam, B. H. Hong, J.-B. Choi, H. R. Choi, *Nanotechnology* **2013**, *24*, 145501.
[4] W. Cai, T. Lai, H. Du, J. Ye, *Sens. Actuators, B Chem.* **2014**, *193*, 492.
[5] C. O. Blattmann, G. A. Sotiriou, S. E. Pratsinis, *Nanotechnology* **2013**, *26*, 8092.
[6] T. Kim, H. Song, J. Ha, S. Kim, D. Kim, S. Chung, J. Lee, Y. Hong, *Appl. Phys. Lett.* **2014**, *104*, 113103.
[7] K. S. Kim, Y. Zhao, H. Jang, S. Y. Lee, J. M. Kim, K. S. Kim, J.-H. Ahn, P. Kim, J.-Y. Choi, B. H. Hong, *Nature* **2009**, *457*, 706.
[8] S. Lim, D. Son, J. Kim, Y. B. Lee, J.-K. Song, S. Choi, D. J. Lee, J. H. Kim, M. Lee, T. Hyeon, D.-H. Kim, *Adv. Funct. Mater.* **2015**, *25*, 375.
[9] P. Görrn, W. Cao, S. Wagner, *Soft Matter* **2011**, *7*, 7177.
[10] M. Amjadi, A. Pichitpajongkit, S. Lee, S. Ryu, I. Park, *ACS Nano* **2014**, *8*, 5154.
[11] H. Wu, D. Kong, Z. Ruan, P.-C. Hsu, S. Wang, Z. Yu, T. J. Carney, L. Hu, S. Fan, Y. Cui, *Nat. Nano* **2013**, *8*, 421.
[12] D. S. Hecht, L. Hu, G. Irvin, *Adv. Mater.* **2011**, *23*, 1482.
[13] D. S. Gray, J. Tien, C. S. Chen, *Adv. Mater.* **2004**, *16*, 393.
[14] C. F. Guo, T. Sun, Q. Liu, Z. Suo, Z. Ren, *Nat. Commun.* **2014**, *5*, 3121.
[15] A. P. Robinson, I. Minev, I. M. Graz, S. P. Lacour, *Langmuir* **2011**, *27*, 4279.
[16] S. Lin, E. K. Lee, M. Khine, *Lab Chip* **2014**, *14*, 3475.
[17] D. Nguyen, D. Taylor, K. Qian, N. Norouzi, J. Rasmussen, S. Botzet, M. Lehmann, K. Halverson, M. Khine, *Lab Chip* **2010**, *10*, 1623.
[18] C. M. Gabardo, Y. Zhu, L. Soleymani, J. M. Moran-Mirabal, *Adv. Funct. Mater.* **2013**, *23*, 3030.
[19] P. P. de Santana, I. M. F. de Oliveira, E. Piccin, *Electrochem. Commun.* **2012**, *16*, 96.
[20] S. Sonney, N. Shek, J. M. Moran-Mirabal, *Biomicrofluidics* **2015**, *9*, 026501.
[21] D. Y. Khang, J. A. Rogers, H. H. Lee, *Adv. Funct. Mater.* **2009**, *19*, 1526.
[22] X. Ho, J. Nie Tey, W. Liu, C. Kweng Cheng, J. Wei, *J. Appl. Phys.* **2013**, *113*, 044311.
[23] J. Zang, S. Ryu, N. Pugno, Q. Wang, Q. Tu, M. J. Buehler, X. Zhao, *Nat. Mater.* **2013**, *12*, 321.
[24] J. A. Rogers, T. Someya, Y. Huang, *Science* **2010**, *327*, 1603.
[25] A. Polywka, T. Jakob, L. Stegers, T. Riedl, P. Görrn, *Adv. Mater.* **2015**, *27*, 3755.
[26] J. Lee, P. Lee, H. Lee, D. Lee, S. S. Lee, S. H. Ko, *Nanoscale* **2012**, *4*, 6408.